# ACTIVE GALACTIC NUCLEUS X-RAY VARIABILITY IN THE *XMM*-COSMOS SURVEY

G. Lanzuisi[1,2], G. Ponti[1], M. Salvato[1,3], G. Hasinger[4], N. Cappelluti[5], A. Bongiorno[6], M. Brusa[1,7], E. Lusso[8],
P. K. Nandra[1], A. Merloni[1,3], J. Silverman[9], J. Trump[10], C. Vignali[7], A. Comastri[5], R. Gilli[5], M. Schramm[9],
C. Steinhardt[8], D. Sanders[4], J. Kartaltepe[11], D. Rosario[1], and B. Trakhtenbrot[12]

[1] Max-Planck-Institut für extraterrestrische Physik, Giessenbachstrasse, D-85748 Garching, Germany; lanzuisi@noa.gr
[2] TUM Fakultät für Physik, James-Franck-Strasse, D-185748 Garching, Germany
[3] Excellence Cluster, Boltzmann Strasse 2, D-85748 Garching, Germany
[4] Institute for Astronomy, 2680 Woodlawn Drive, Honolulu, HI 96822-1839, USA
[5] INAF-Osservatorio Astronomico di Bologna, via Ranzani 1, I-40127 Bologna, Italy
[6] Istituto Nazionale di Astrofisica-Osservatorio Astronomico di Roma Via Frascati 33, I-00040, Monte Porzio Catone, Italy
[7] Dipartimento di Fisica e Astronomia, Università di Bologna, viale Berti Pichat 6/2, I-40127 Bologna, Italy
[8] Max Planck Institut für Astronomie, Königstuhl 17, D-69117 Heidelberg, Germany
[9] Kavli Institute for the Physics and Mathematics of the Universe (Kavli IPMU) 5-1-5 Kashiwanoha Kashiwa, Chiba 277-8583, Japan
[10] University of California Observatories/Lick Observatory and Department of Astronomy and Astrophysics, University of California, Santa Cruz, CA 95064, USA
[11] National Optical Astronomy Observatory, 950 North Cherry Avenue, Tucson, AZ 85719, USA
[12] Wise Observatory, Tel Aviv University, 69978 Tel Aviv, Israel

## ABSTRACT

We used the observations carried out by *XMM* in the COSMOS field over 3.5 yr to study the long term variability of a large sample of active galactic nuclei (AGNs) (638 sources) in a wide range of redshifts ($0.1 < z < 3.5$) and X-ray luminosities ($10^{41} < L_{0.5-10} < 10^{45.5}$). Both a simple statistical method to assess the significance of variability and the Normalized Excess Variance ($\sigma_{rms}^2$) parameter were used to obtain a quantitative measurement of the variability. Variability is found to be prevalent in most AGNs, whenever we have good statistics to measure it, and no significant differences between type 1 and type 2 AGNs were found. A flat (slope $-0.23 \pm 0.03$) anti-correlation between $\sigma_{rms}^2$ and X-ray luminosity is found when all significantly variable sources are considered together. When divided into three redshift bins, the anti-correlation becomes stronger and evolving with $z$, with higher redshift AGNs being more variable. We prove, however, that this effect is due to the pre-selection of variable sources: when considering all of the sources with an available $\sigma_{rms}^2$ measurement, the evolution in redshift disappears. For the first time, we were also able to study long term X-ray variability as a function of $M_{BH}$ and Eddington ratio for a large sample of AGNs spanning a wide range of redshifts. An anti-correlation between $\sigma_{rms}^2$ and $M_{BH}$ is found, with the same slope of anti-correlation between $\sigma_{rms}^2$ and X-ray luminosity, suggesting that the latter may be a by-product of the former. No clear correlation is found between $\sigma_{rms}^2$ and the Eddington ratio in our sample. Finally, no correlation is found between the X-ray $\sigma_{rms}^2$ and optical variability.

*Key words:* galaxies: active – X-rays: galaxies – X-rays: general

*Online-only material:* color figures

## 1. INTRODUCTION

Variability, in time scales from minutes to years, is one of the defining characteristics of black hole (BH) accretion. Indeed, the rapid variability of quasars was one of the arguments for the presence of a compact central engine powering these sources (Rees 1984).

Variability has long been used as an AGN selection technique in the optical (van den Bergh et al. 1973; Bonoli et al. 1979; Giallongo et al. 1991; Trevese et al. 1994; Vanden Berk et al. 2004; de Vries et al. 2005). More recently, optical variability has been used to select AGNs (typically low luminosity AGNs) in X-ray and multi-wavelength surveys, complementing other selection techniques (Trevese et al. 2008; Villforth et al. 2010; Sarajedini et al. 2011; Young et al. 2012).

In X-rays, the first results from *EXOSAT* and *RXTE* showed that the variability amplitude is anti-correlated with X-ray luminosity, and that the power spectral density (PSD) can be modeled with a power law with a slope steeper than 1, i.e., the variability decreases with increasing frequency (Barr & Mushotzky 1986; Lawrence & Papadakis 1993; Green et al. 1993; Nandra et al. 1997; Markowitz & Edelson 2004).

The combination of these results with short term, high quality light curves with *XMM-Newton* for a handful of AGNs, has allowed the study of the PSD in a larger range of frequencies. As previously suggested (Papadakis & McHardy 1995), the steep PSD flattens below a break frequency $\nu_b$ (Edelson & Nandra 1999; Uttley et al. 2002; Markowitz & Edelson 2004). A similar behavior is observed in galactic BH binaries (BHBs, e.g., Axelsson et al. 2005; Gierliński et al. 2008). This suggests that similar processes are in place for these two classes of sources, with the difference in time scales related to the different BH mass ($M_{BH}$) ranges involved. Thus, the variability–luminosity relation could be a consequence of an intrinsic variability–BH mass relation (Hayashida et al. 1998; Czerny et al. 2001; Papadakis 2004).

McHardy et al. (2006) demonstrated that, as far as variability is concerned, supermassive BHs (SMBHs) are scaled versions of BHBs and that, over eight orders of magnitude in $M_{BH}$ and six in frequency, the $\nu_b$ is inversely correlated with the BH mass, once corrected for different accretion rates. Körding et al. (2007) proposed a direct correlation between $\nu_b$, $M_{BH}$, and accretion rate ($\dot{M}$), where $\nu_b$ scales linearly with both $\dot{M}$ and $M_{BH}^{-1}$ (but see also González-Martín & Vaughan 2012).

For variability studies, the PSD is a powerful tool but long, uninterrupted light curves for AGNs are difficult to achieve and are available only for a handful of local sources. The normalized excess variance $\sigma_{rms}^2$ has been used as a more convenient tool for sparse sampling of light curves in large AGN samples. Nandra et al. (1997), Turner et al. (1999), and George et al. (2000) applied this technique to *ASCA* data, for both quasars and Seyferts, finding an anti-correlation of $\sigma_{rms}^2$ with X-ray luminosity and $M_{BH}$, and a correlation with X-ray spectral index. O'Neill et al. (2005) used *ASCA* light curves of 46 local AGNs to study the correlation with $M_{BH}$ (and $L_{2-10}$). Zhou et al. (2010) found, on a sample of local AGNs with available reverberation mapping BH masses, a tight correlation between $\sigma_{rms}^2$ and $M_{BH}$, proposing it as a method to infer the BH mass from $\sigma_{rms}^2$. Using a sample of 161 local (mostly at $z < 0.2$) AGNs (every X-ray unabsorbed radio quiet AGN observed by *XMM* in pointed observations), Ponti et al. (2012, hereafter P12) found that, to first approximation, all local AGNs have the same variability properties once rescaled for $M_{BH}$ (and $\dot{M}$). The authors measured a tight correlation between $\sigma_{rms}^2$ and $M_{BH}$, with the scatter becoming smaller (only a factor of 2–3, comparable to the one induced by the $M_{BH}$ uncertainties) when the subsample of reverberation mapped AGNs was considered (see also Kelly et al. 2011). This suggests that X-ray variability $M_{BH}$ measurements are more accurate than those based on single epoch optical spectra. A highly significant correlation between $\sigma_{rms}^2$ and 2–10 keV spectral index was also observed.

All of these studies are based on local AGN and short time scale light curves (typically from minutes to days), i.e., in a range of frequencies typically above $\nu_b$. Given that $\sigma_{rms}^2$ roughly measures the integral of the PSD over the sampled time scales, the shift of $\nu_b$ with the BH mass is thought to produce the correlation between the observed variability and $M_{BH}$.

On longer time scales, therefore at $\nu \ll \nu_b$, the PSD has only been measured for a few AGNs. In particular, the normalization of the flat portion of the PSD is not well know. It is generally assumed that this normalization is the same for all AGNs, regardless of the BH mass and luminosity (e.g., Papadakis 2004), as recently observed on very long time scale *RXTE* light curves for a small sample of local AGNs (Zhang 2011). The $\nu_b$ for a BH mass of $10^9 M_\odot$ is of the order of 1 yr, so very long observations/samplings are required to investigate this frequency range.

This range of frequencies is becoming accessible for a large sample of sources in deep X-ray surveys, where a large total exposure is achieved through repeated observations over several years. They are able to detect variability in moderate luminosity or high redshift AGNs (e.g., Paolillo et al. 2004 for CDF-S, Papadakis et al. 2008 for Lockman Hole data). Young et al. (2012) utilized X-ray variability to select elusive AGNs (finding 20 new AGN candidates), using the 4 Ms of *Chandra* exposure in the CDF-S, taken over 10.8 yr.

In this paper we use the repeated observations performed with *XMM-Newton* to cover the 2 deg$^2$ field of the Cosmic Evolution Survey (COSMOS) (Scoville et al. 2007), with 55 pointings from 2003 December to 2007 May and a total of 1.5 Ms of exposure (Hasinger et al. 2007), to study the long term variability of the entire catalog of X-ray detected sources (Cappelluti et al. 2009). The catalog has an almost 100% completeness in optical/IR identification (Brusa et al. 2010). The availability of spectroscopic redshifts or reliable photometric redshifts allows us to study the X-ray variability as a function of spectral type, luminosity, and redshift. Most (~800) of our sources have a $L_{Bol}$

estimate from spectral energy distribution (SED) fitting (Lusso et al. 2011, 2012), and a BH mass estimate, either from optical broad line (BL) for type 1 (Trump et al. 2009; Merloni et al. 2010; Matsuoka et al. 2013), or from scaling relations for type 2 (Lusso et al. 2011), allowing us to study the dependency of the variability also as a function of BH mass and accretion rate.

The paper is organized as follows. Section 2 summarizes the properties of the data set and the extraction of light curves. Section 3 presents the variability estimator $V$, while Section 4 introduces the Normalized Excess Variance ($\sigma_{rms}^2$). In Section 5 the distributions of $\sigma_{rms}^2$ as a function of $L_{0.5-10}$, $z$, $M_{BH}$, Eddington ratio, and optical variability are discussed and Section 6 summarizes the results. A standard $\Lambda$ cold dark matter cosmology with $H_0 = 70$ km s$^{-1}$ Mpc$^{-1}$, $\Omega_\Lambda = 0.73$, and $\Omega_M = 0.27$ is assumed throughout the paper. Errors are given at the $1\sigma$ confidence level for one interesting parameter, unless otherwise specified.

## 2. DATA SET

### 2.1. The COSMOS Survey

COSMOS is a deep and wide extragalactic survey designed to probe the formation and evolution of galaxies as a function of cosmic time and large-scale structural environment. The survey covers a 2 deg$^2$ equatorial ($10^h$, +02°) field with imaging by most of the major space-based telescopes (*Hubble Space Telescope* (*HST*), *Spitzer*, *Galaxy Evolution Explorer*, *XMM-Newton*, *Chandra*), and a number of large ground based telescopes (Subaru, Very Large Array, European Southern Observatory Very Large Telescope (ESO-VLT), UKIRT, NOAO, Canada–France–Hawaii Telescope (CFHT), and others). Large dedicated ground-based spectroscopy programs in the optical with Magellan/IMACS (Trump et al. 2007), VLT/VIMOS (Lilly et al. 2009), Subaru-FMOS, and DEIMOS-Keck have been completed or are well under way.

This wealth of data has resulted in an 35-band photometric catalog of ~$10^6$ objects (Capak et al. 2007) resulting in photo-$z$ for the galaxy population accurate to $\Delta z/(1 + z) < 1\%$ (Ilbert et al. 2009) and to $\Delta z/(1 + z) \sim 1.5\%$ for the AGN population (Salvato et al. 2009, 2011).

### 2.2. XMM-COSMOS

The *XMM-Newton* wide-field survey in the COSMOS field (hereafter *XMM*-COSMOS; Hasinger et al. 2007) is a crucial component of the multi-wavelength coverage of the COSMOS field. The ~2 deg$^2$ area of the *HST*/Advanced Camera for Surveys program has been surveyed with *XMM-Newton* for a total of ~1.55 Ms during the AO3, AO4, and AO6 cycles of *XMM* observations, providing an unprecedented large sample of point-like X-ray sources (~1800).

The *XMM*-COSMOS project is described in Hasinger et al. (2007, hereafter Paper I), while the X-ray point source catalog and counts from the complete *XMM*-COSMOS survey are presented in Cappelluti et al. (2009, hereafter Paper II). Brusa et al. (2010, hereafter Paper III) present the optical identifications of the X-ray point sources in the *XMM*-COSMOS survey and the multi-wavelength properties of this large sample of X-ray selected AGNs.

The catalog used in this work includes 1797 point-like sources detected in the 0.5–2 (1545 sources), 2–8 (1078 sources), and 4.5–10 (246 sources) keV bands. The nominal limiting fluxes are ~$5 \times 10^{-16}$, ~$3 \times 10^{-15}$, and ~$7 \times 10^{-15}$ erg cm$^{-2}$ s$^{-1}$,

respectively. The adopted likelihood threshold corresponds to a probability $4.5 \times 10^{-5}$ that a catalog source is a spurious background fluctuation. In this analysis, we used the source list created from the 53 *XMM*-COSMOS fields.

The *XMM*-COSMOS catalog has almost 100% redshift completeness (Paper III). 884 (out of 1797) sources have a spectroscopic redshift, 748 sources have a photometric redshift, 97 are classified as stars, and 68 remain unclassified. The sources with spectroscopic redshift are divided almost equally between BL (FWHM > 2000 km s$^{-1}$) and non-BL AGNs, plus a small fraction of non AGN sources, i.e., passive galaxies at low redshift or stars. The sources for which only photometric redshift is available have been classified on the basis of the best SED fitting template. The agreement between SED classification and spectral classification is good (Lusso et al. 2010; Salvato et al. 2009; Brusa et al. 2010). The final classification breakdown is: 611 type 1, 941 type 2, 80 Galaxies, 97 Stars, and 68 Unclassified.

We underline that in the following analysis type 1 refers to sources that either have a spectroscopic redshift, showing at least one broad emission line, or have as best fit SED templates an unobscured quasar template with different degrees of contamination by star-forming galaxy templates (from 10% to 90% of the optical–near-IR flux). Type 2 refers to sources with optical spectra of narrow lines AGNs or passive/star-forming galaxies, or best fit SED templates of obscured AGNs, with different degrees of contamination by passive or star-forming galaxy templates. We exclude sources classified as stars and those which are unclassified from the following analysis.

### 2.3. Light Curve Extraction

Because of the pattern of observations, sources in *XMM*-COSMOS can be observed in a minimum of one to a maximum of 11 pointings. We have the possibility of following up every source for a period of up to 3.5 yr.

By using the *XMM*-SAS tool *emldetect*, we selected all sources with a detection significance $det_{ml} > 10$ (corresponding to a probability that a Poissonian fluctuation of the background is detected as a spurious source of $P = 10^{-10}$), in each pointing. We then produced light curves of all those sources observed in more than one pointing. As a result, we produced light curves for 995 of the 1797 sources in the full band catalog. The number of detections spans from two to nine, depending on the position of the source and on its flux. Figure 1 (left panel) shows the distribution of all of the detections of sources in the total catalog, during the 3.5 yr observing campaign (between 2003 December 6 and 2007 May 18). We have a total of 3849 single detections, distributed among the observations depending on the exposure time of each pointing. In order to study variability in these sources, we limited the following analysis to sources with $\geqslant 3$ or more detections.

To obtain an estimate of the typical rest-frame time scales sampled by the available 3.5 yr observing campaign, we computed the time intervals between the first and the last detections for each source, rescaled for the redshift of the source, for time dilation, i.e., $\Delta t_{\rm rest} = \Delta t/(1+z)$. Figure 1 (right panel) shows the distribution of the time intervals for all of the 638 sources with $\geqslant 3$ detections. The inset shows the distribution of the number of detections for each source in the sample: 190 sources have only three detections in total and in the last bin we have ten sources with nine detections, which is the maximum number of samplings available. The plot shows that, given the distribution of the observations and the redshift distribution of the sources, the vast majority of the light curves have a total length in the
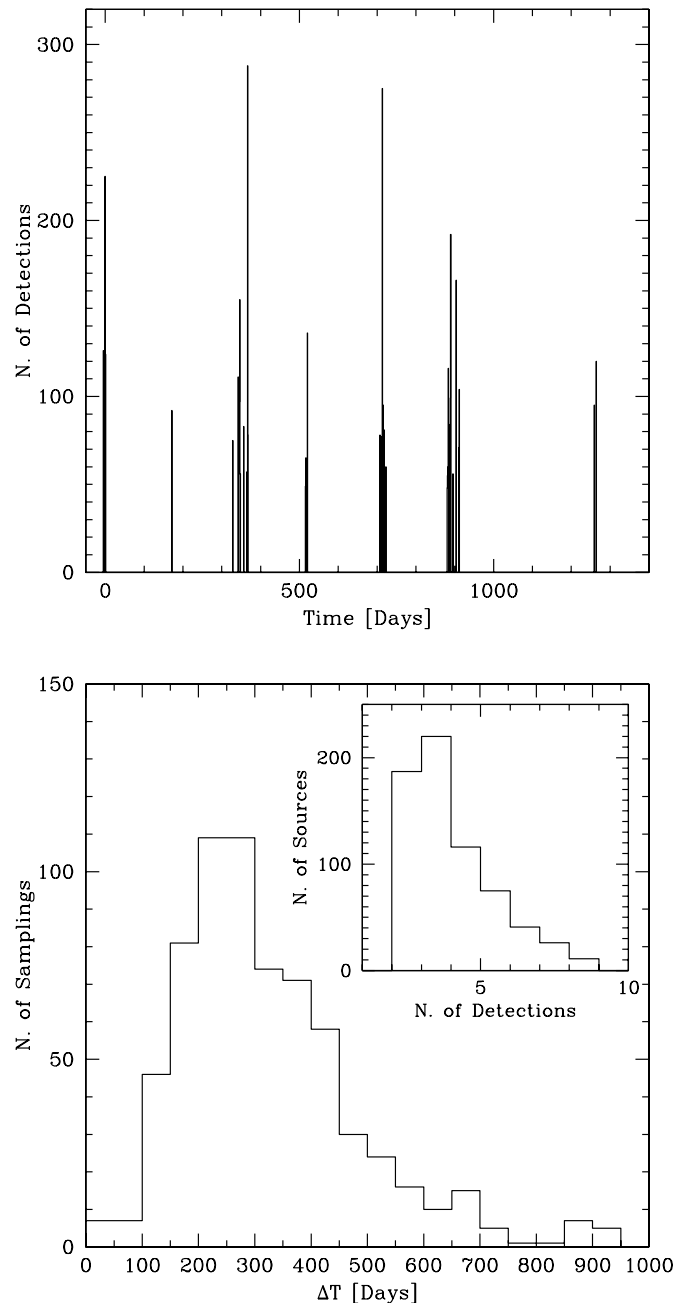


**Figure 1.** Top panel: distribution of single source detections, during the 3.5 yr observing campaign (between 2003 December 6 and 2007 May 18). Bottom panel: distribution of the total light curve length, rescaled for the redshift of the source, for all of the sources. The inset shows the distribution in number of detections for the sources in our sample.

range of 100–500 days (rest-frame), i.e., the low frequency limit of the light curve is typically at frequencies lower than $\nu_b$ for most of our sources. As a point of reference, we recall that the typical break frequency in the PSD of an AGN with a $10^8 M_\odot$ BH is $1/\nu_b \sim 30$ days. The final breakdown of sources with light curves is 340 type 1, 291 type 2, and seven galaxies.

The light curves are measured in the fixed 0.5–10 keV observed band, implying that we are measuring variability at increasingly high intrinsic energies, up to 2–40 keV at $z = 3$. Even if variability can, in principle, be highly energy dependent, given the different spectral components (with different origins) which observationally dominate different bands, it is known to be well correlated between the 0.3–0.7, 0.7–2, and 2–10 keV bands

(e.g., P12). In soft X-rays the effect of observing variability in different bands is small: typically ∼10% from 0.5 to 10 keV for local Seyferts (Vaughan & Fabian 2004; Gallo et al. 2007). In hard X-rays (above 10 keV) less data are available. However, Caballero-Garcia et al. (2012) found that the variability amplitude above 10 keV is similar to that below 10 keV for a sample of five bright AGNs in the *Swift*-BAT 58 month catalog (see also Beckmann et al. 2008; Soldi et al. 2011). Soldi et al. (2013, submitted) reported for a sample of 110 radio quiet QSO from the same *Swift*-BAT 58 month catalog, that the variability is very well correlated even between the 14–24 and 35–100 keV bands (again with a 10% difference).

Furthermore, all of the variability estimators are strongly dependent on the available number of counts (see Section 3), hence we decided to exploit all of the X-ray counts available using the full *XMM-Newton* observing band for all sources, instead of restricting ourselves to a much narrower fixed rest-frame band. It is true, however, that we do not know if the variability is energy dependent in AGNs at high redshift, contrary to what is observed in the local universe. To answer this question, however, one needs a large sample of sources spanning a large redshift range, which are not so severely affected by low signal-to-noise ratio (S/N). The almost uniform 200 ks *Chandra* coverage on the entire 2 deg² COSMOS field, which will be available by the end of 2013, will be the perfect data set for such a study.

## 3. THE *V* PARAMETER

To obtain an estimate of the probability of variability for each source, we adopted the method described in McLaughlin et al. (1996) and also used in Paolillo et al. (2004) and Young et al. (2012). To statistically quantify the variability of the sources, we computed

$$\chi^2 = \sum_{i=1}^{N_{obs}} \frac{(x_i - \overline{x})^2}{\sigma_{err,i}^2}, \quad (1)$$

where $N_{obs}$ is the number of pointings in which the source was detected, $x_i$ is the flux of the source in each pointing, $\sigma_{err,i}^2$ is the error, and $\overline{x}$ is the average flux. For intrinsically non-variable sources the value of $\chi^2$ is expected to be ∼$N_{obs} - 1$ (i.e., $\chi^2/dof = 1$). To determine whether the $\chi^2$ value is consistent with flux variability, we computed the probability $P(\chi^2)$ that a $\chi^2$ lower than the observed could occur by chance for an intrinsically non-variable source. We then define the variability index $V = -\log(1 - P)$ to synthetically express the strength of evidence of variability (i.e., $V = 1$ corresponds to 90% confidence, $V = 1.3$%–95%, $V = 2$%–99%, and so on). A typical value for the critical probability $P_{crit}$, used to discriminate between variable and non-variable sources in previous works with comparable sampling (but with smaller samples of AGNs), is 95% (Paolillo et al. 2004; Papadakis et al. 2008; Young et al. 2012). Following this approach, we selected sources with $V > 1.3$ ($P_{crit} = 95\%$), i.e., sources that have only a 5% probability that the variability observed is due to Poisson noise alone and the source is intrinsically non-variable. This translates into a sample of 232 variable sources, with an expected number of false positive of ∼32. Adopting a more conservative approach and selecting sources with $V > 2$ ($P_{crit} = 99\%$), we would select a smaller sample of variable sources (164) with a smaller number of false positive (∼7). This would eliminate ∼25 false positives but it would also miss a similar amount of truly variable sources. We stress, however, that we verified that

using the sample selected with the more conservative approach ($V > 2$), produces very similar results to the ones presented in the following, only with a smaller sample and thus larger uncertainties.

### 3.1. V versus Counts

The *V* parameter is strongly dependent on the number of counts available, given that the ability to constrain the variability of one source depends on the error on each measurement. Figure 2 (left panel) shows the distribution of the *V* parameter as a function of the total number of counts for each source. In Figure 2 (right panel) we show the fraction of variable sources ($V > 1.3$) in bins of 0.5–10 keV counts. The fraction decreases from ∼75% ± 13% above 1000 counts, to ∼15% ± 10% in the last bin, i.e., given sufficient statistics to detect it, variability is almost ubiquitous in X-ray selected AGNs. However, even at a very high number of counts, a small fraction of sources is found to be non-variable with high reliability.

In Figure 2 (top) three sources are highlighted, namely *XMM-Newton* ID (XID) 3, 5323, and 2186. The X-ray and optical light curves for these sources are shown in the Figure 3 upper and lower panels, respectively, (optical light curves from M. Salvato et al. 2013, in preparation) Each one represents one extreme of the distribution: source 3 has the highest number of X-ray counts (and the maximum number of detections, nine) and is highly variable, both in X-ray and optical; source 5323 again has very good X-ray statistics, but is non-variable with very high confidence (only a 5% probability of being variable) and is also non-variable in optical; source 2186 has a more typical number of counts for our sample (∼200 net counts in 0.5–10 keV) and is variable, both in X-ray and optical. Sources 5323 and 2186 have the same observed light curve duration, while source 3 was detected during the entire 3.5 yr of observations. However source 5323 is a luminous quasar at high $z$ ($\log(L_X) = 45.4$ and $z = 1.509$, with $\log(M_{BH}) = 8.9$), while 2186 is a low luminosity Seyfert at low redshift ($\log(L_X) = 42.1$ and $z = 0.235$, with $\log(M_{BH}) = 7.3$). As we will show in Section 5, the different luminosities (and $M_{BH}$) appear to have a major role in producing these different variability properties.

In total, 232 of 638 sources (36.4% of the sample) exhibit significant flux variability on rest-frame time scales of months to years. We can compare this result with those of Young et al. (2012) on CDF-S *Chandra* data. They found 50% of AGNs to be variable. This difference is probably due to the different background contribution for *Chandra* and *XMM-Newton*: for a given total number of net counts, the S/N and hence the error on the flux measurement is typically lower (with larger errors) for *XMM-Newton* data. The *Chandra* background accounts for only 5%–10% of source counts even for faint sources, while the background for faint sources in the *XMM-Newton*-COSMOS survey can account for up to 50% of source counts in the full band.

### 3.2. V versus $L_{0.5-10}$ and z

We are interested in the possible correlation between X-ray variability and more intrinsic properties of the sources in our sample, such as $L_{0.5-10}$ and redshift. However, the strong dependency of *V* on the number of counts could produce biased correlations between these quantities. We therefore explored the distribution of $L_{0.5-10}$ and redshift as a function of the number of counts (Figure 4 left and right, top panels), for the whole sample (gray points) and for variable sources ($V > 1.3$, black points).
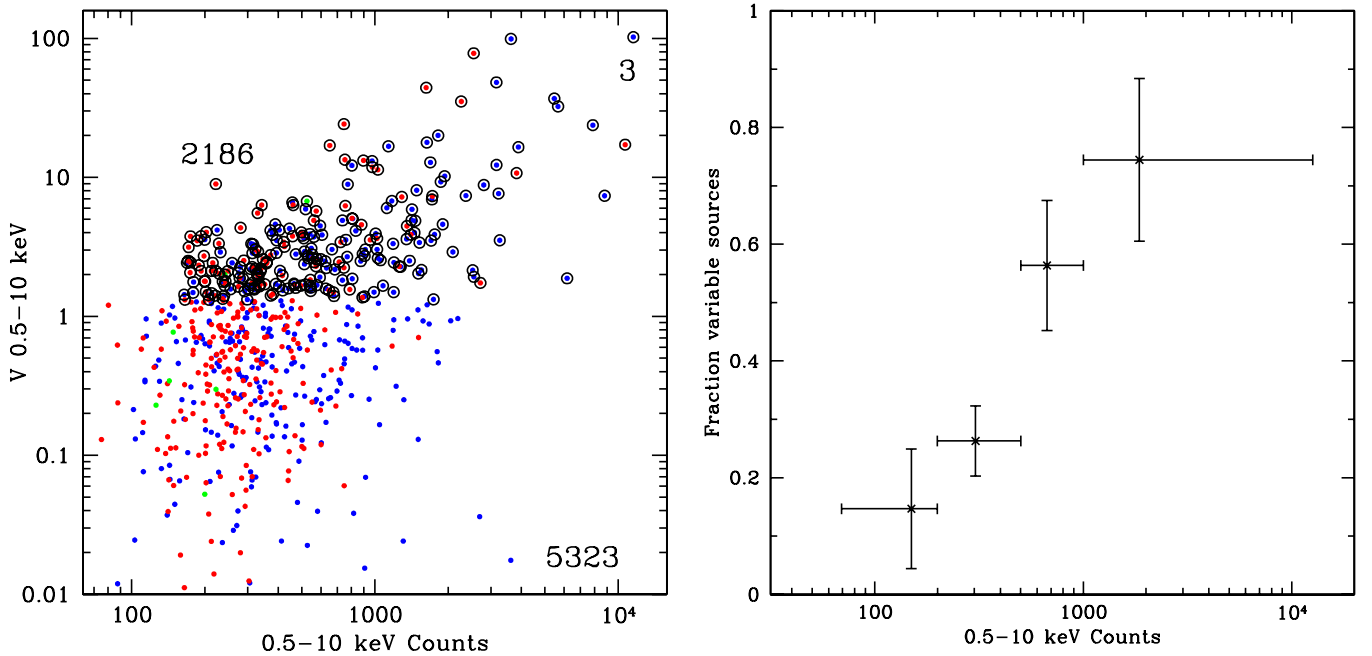
**Figure 2.** Left panel: distribution of $V$ parameter as a function of 0.5–10 keV net counts. Blue represents type 1, red type 2 and green galaxies. Sources with $V > 1.3$ are labeled with black circles. This corresponds to a source being variable at a 95% confidence level. Three peculiar sources are labeled with their XID number. Their X-ray and optical light curves are shown in Figure 3. Right panel: fraction of variable sources ($V > 1.3$) as a function of number of counts in bins of counts.
(A color version of this figure is available in the online journal.)

The resulting fraction of variable sources in bins of $L_{0.5-10}$ and $z$ is show in the lower panels.

In Figure 4 (top) there is a clear upper boundary in the distribution of the luminosities ($L_{0.5-10} \sim 5 \times 10^{45}$ erg s$^{-1}$) due to the angular size of the COSMOS survey and the low density of very luminous AGNs and a lower boundary in the number of counts ($\sim 50$) due to the detection threshold of each observation and the minimum number of detections of three. Furthermore, it can be seen that there is a general decreasing density of sources toward low luminosities, due to the smaller volume sampled at low $z$. Finally there is a zone of missing sources at low luminosities and a high number of counts due to the typical exposure time of the survey ($\sim 40$ ks vignetting corrected). However, the fraction of variable sources (i.e., the relative distribution of variable and non-variable sources) is constant, close to 40%, in the entire $L_{0.5-10}$ range we considered ($10^{41} < L_{0.5-10} < 5 \times 10^{45}$ erg s$^{-1}$).

The distribution of counts as a function of redshift is shown in Figure 4 (bottom). Here the zone of missing sources at high redshift and a high number of counts is again due to the properties of the survey (exposure time and angular size): there are no sources more luminous than $5 \times 10^{45}$ erg s$^{-1}$ and the almost constant exposure time dictates a decreasing number of counts with z. In this case, however, the final effect is a decrease in the fraction of variable sources at high redshift, from 55% to 25% from low to high redshift.

We stress that the distribution of the $V$ parameter is an indicator of our ability to detect variability in our sample and therefore Figure 4 (bottom) gives an indication that we are less able to detect and measure variability at high $z$ (see discussion in Section 5).

### 3.3. V versus Optical Type

Figure 5 (left panel) shows the distribution of the variability parameter, $V$, for the 638 sources with an available light curve in the 0.5–10 keV band, divided by class. The dashed line represents the probability threshold we choose to define a source as variable. Figure 5 (right panel) shows the fraction of variable sources for the different classes. Type 1 AGNs have the highest fraction of variable sources ($\sim 40\%$), type 2 have a lower fraction ($\sim 32\%$), while galaxies have only a very large upper limit (only one variable source out of seven in this class). The inset of Figure 5 (bottom) shows, however, that the higher fraction of variable type 1 (with respect to type 2 sources), could be due to the typical higher number of counts available for these sources. Therefore, as observed also in the CDF-S (Young et al. 2012) variability is common in AGN samples, independent of the optical classification.

### 4. THE EXCESS VARIANCE $\sigma^2_{\rm rms}$

To obtain a quantitative measure of the variability amplitude, we calculated the normalized excess variance ($\sigma^2_{\rm rms}$; Nandra et al. 1997; Turner et al. 1999) for all of the 638 sources with more than two detections. The normalized excess variance is defined as:

$$\sigma^2_{\rm rms} = \frac{1}{(N_{\rm obs} - 1)\overline{x}^2} \sum_{i=1}^{N_{\rm obs}} (x_i - \overline{x})^2 - \frac{1}{N_{\rm obs}\overline{x}^2} \sum_{i=1}^{N_{\rm obs}} \sigma^2_{{\rm err},i}, \quad (2)$$

where $N_{\rm obs}$ is the number of observations, $\overline{x}$ is the average flux, and $x_i$ is the single measurement with error $\sigma_{{\rm err},i}$. $\sigma^2_{\rm rms}$ measures how much of the total flux per observation is variable after subtracting the statistical error. Note that this form is usually simplified using the factor $1/N_{\rm obs}$ in both terms, which gives consistent results for a large number of observations. Instead, given the typically small number of observations available in our case, the difference between $N$ and $N - 1$ is significant.
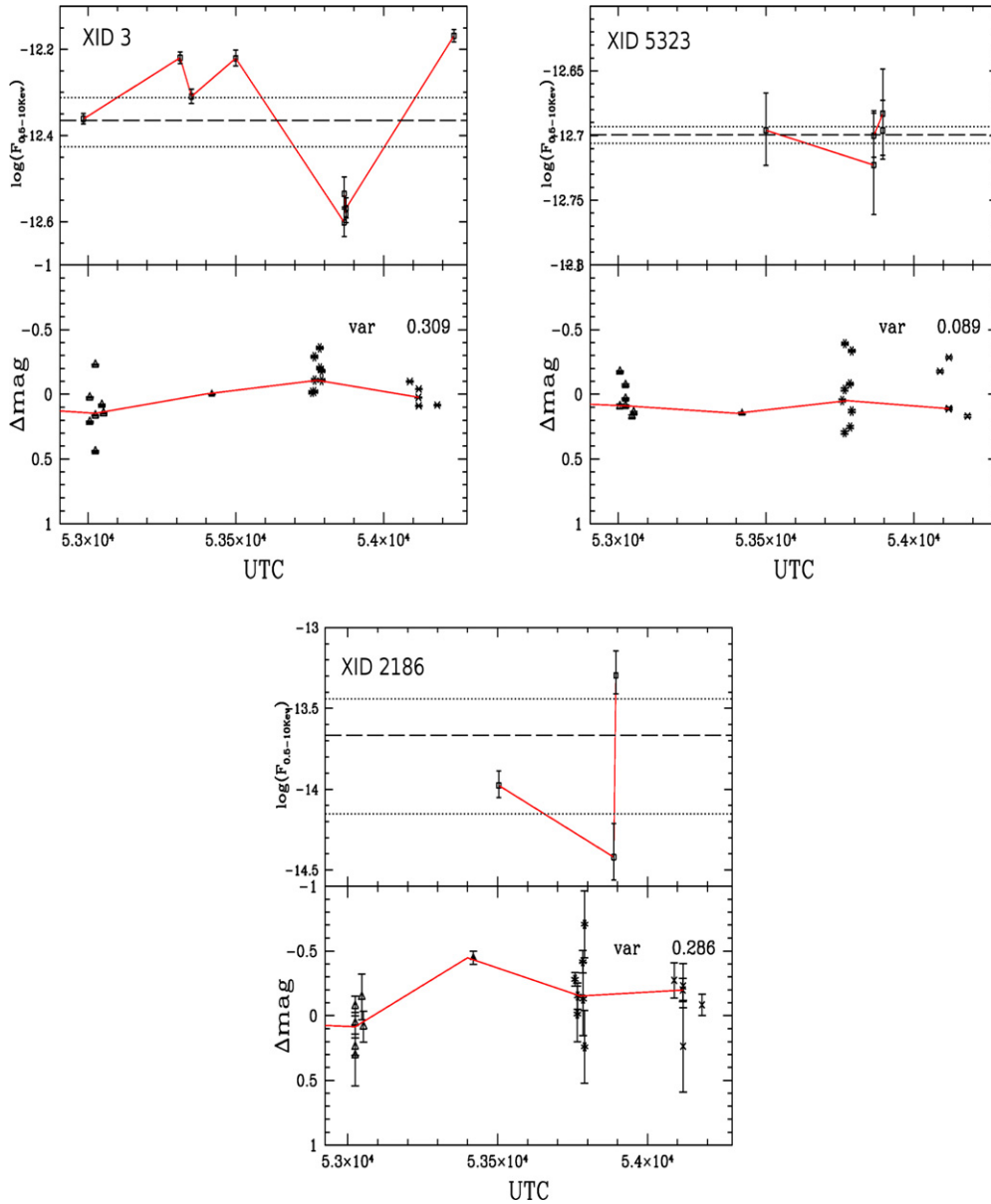
**Figure 3.** X-ray (top) and optical (bottom) time variability for the sources XID 3, 5323, and 2186, respectively. Top panels: the dashed line shows the weighted mean of the 0.5–10 keV flux. Dotted lines show the standard error on the mean. The continuous line connects data points. Bottom panels: the sources was observed in four epochs, each epoch marked with a different symbol. The four groups are, from left to right: Subaru broad-band images (Subaru$_{BB}$), CFHT$g$ band, the first set of intermediate bands Subaru images (Subaru$_{IB1}$), and the second epoch of intermediate bands Subaru images (Subaru$_{IB2}$). The red line connects the median values of the deviation from a running Gaussian filter for each group of observations. The points in each group refer to different wavelengths, therefore the differences within points in each group are due to the SED shape and not variability. More details on the optical variability are available in Salvato et al. (2009).
(A color version of this figure is available in the online journal.)

The error on the excess variance due to Poisson noise is given by Vaughan et al. (2003; see also Ponti et al. 2004):

$$\mathrm{err}(\sigma_{\mathrm{rms}}^2) = \sqrt{\left(\sqrt{\frac{2}{N_{\mathrm{obs}}}} \cdot \frac{\overline{\sigma_{\mathrm{err}}^2}}{\overline{x}^2}\right)^2 + \left(\sqrt{\frac{\overline{\sigma_{\mathrm{err}}^2}}{N_{\mathrm{obs}}}} \cdot \frac{2F_{\mathrm{var}}}{\overline{x}}\right)^2} \quad (3)$$

where $\overline{\sigma_{\mathrm{err}}^2}$ is the mean square error:

$$\overline{\sigma_{\mathrm{err}}^2} = \frac{1}{N_{\mathrm{obs}}} \sum_{i=1}^{N} \sigma_{\mathrm{err},i}^2 \quad (4)$$

and $F_{\mathrm{var}}$ is the fractional variability (Edelson et al. 1990), $F_{\mathrm{var}} = \sqrt{\sigma_{\mathrm{rms}}^2}$.

If the intrinsic excess variance is consistent with zero, due to statistical fluctuations, the measured $\sigma_{\mathrm{rms}}^2$ can be negative. We consider it as a "detection" if $\sigma_{\mathrm{rms}}^2$-err($\sigma_{\mathrm{rms}}^2$) > 0, (there are 228 sources in our sample with such "detections"). For the remaining 410 sources, we define an "upper limit" (UL) to the measured excess variance as: UL = $\sigma_{\mathrm{rms}}^2$ + err($\sigma_{\mathrm{rms}}^2$). We emphasize that in the following we will use these ULs for the fit with the survival analysis, but we also tested that consistent results are obtained if $3\sigma$ ULs are used instead.

It is well known that, apart from the Poisson noise, there are other sources of uncertainties in the determination of excess variance related to the intrinsic scatter of the variability and to the sampling of the light curves, which become even more important for sparsely sampled light curves.
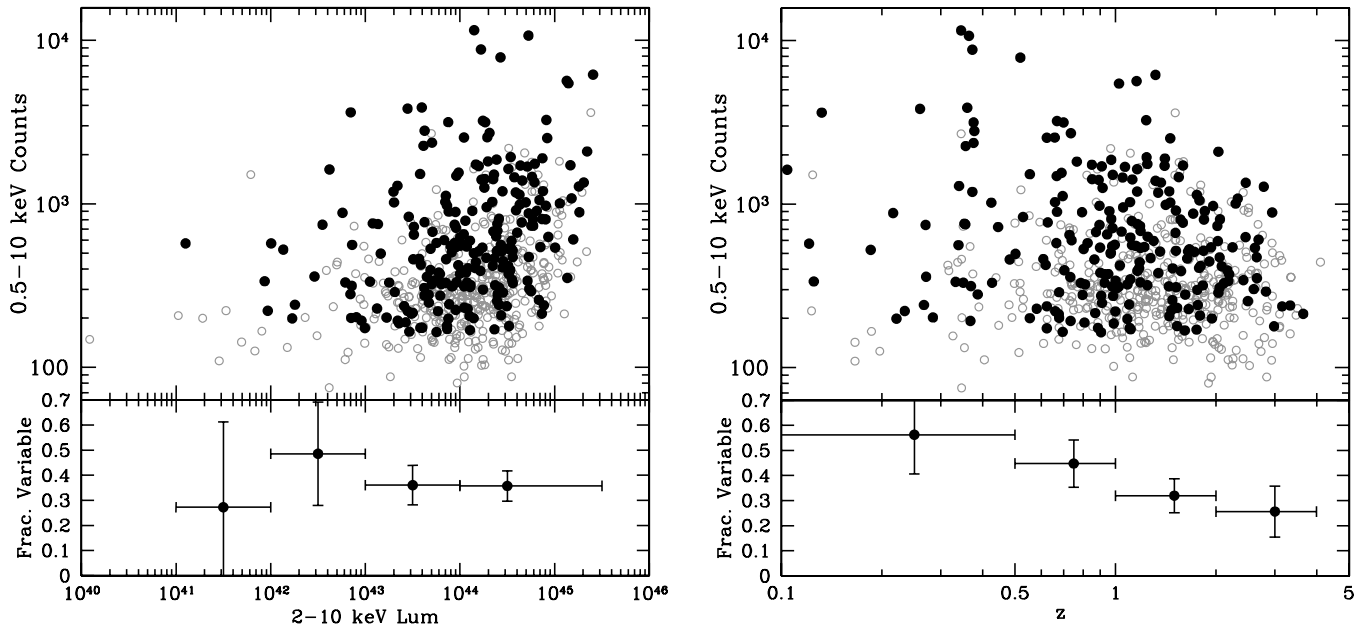
**Figure 4.** Left panel: distribution of 0.5–10 keV intrinsic luminosity as a function of 0.5–10 keV net counts (top). Sources with $V > 1.3$ are labeled in black. The fraction of variable sources in bins of $L_{0.5-10}$ is shown in the lower panel. Vertical error bars represent the Poissonian error on the measurement, horizontal error bars show the bin size. Right panel: same as left panel, but as a function of redshift.
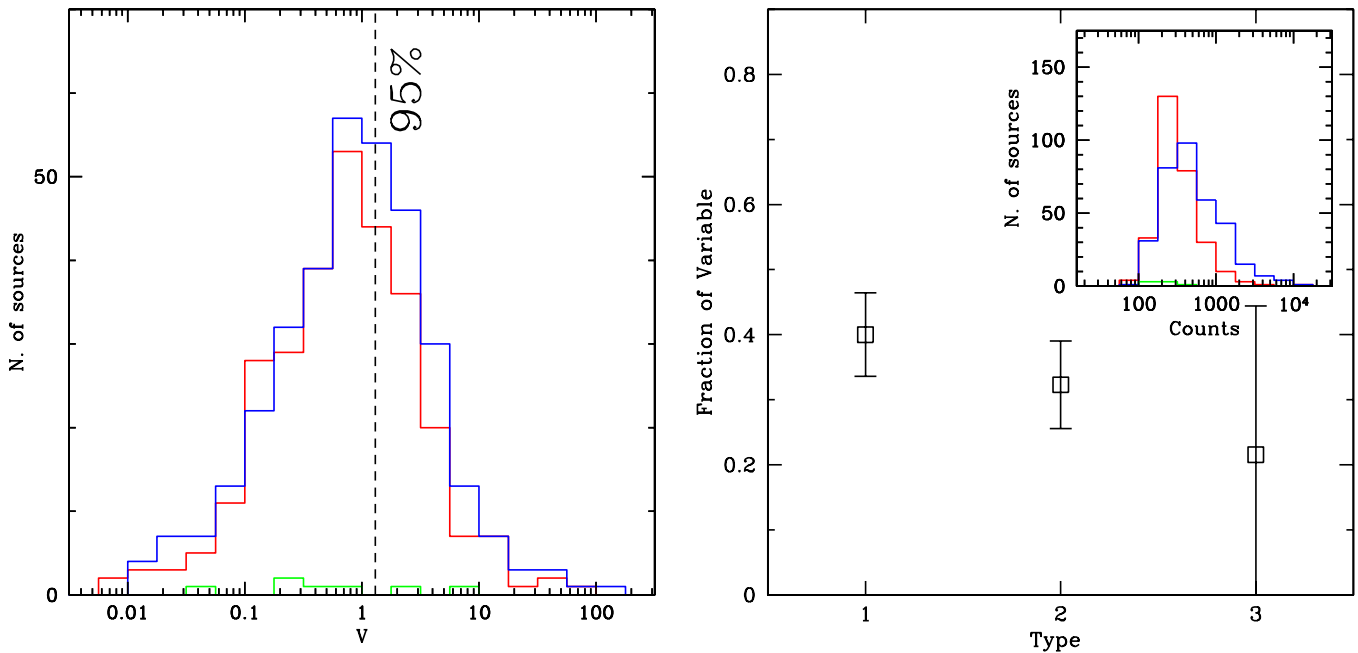


**Figure 5.** Left panel: distribution of the variability parameter $V$, for the 638 sources with available light curves in the 0.5–10 keV band, divided by class. Type 1 AGNs are shown in blue, type 2 AGNs in red, and galaxies in green. Right panel: fraction of variable source ($V > 1.3$) for the different classes: 1 for type 1, 2 for Type 2, and 3 for galaxies. The inset shows the distribution of counts per type of sources, colors are the same as in the left panel.

(A color version of this figure is available in the online journal.)

Allevato et al. (2013) showed through Monte Carlo simulations that the values of the excess variance, measured from either continuously or sparsely sampled light curves, differ from the intrinsic, band normalized, excess variance. In the case of sparsely sampled light curves, the measured $\sigma_{\rm rms}^2$ is typically an underestimate of the intrinsic $\sigma_{\rm rms}^2$ because of the frequencies that are not well sampled. The bias factor[13] of a single measure-

ment depends on the slope of the PSD, $\beta$, on the light curve sampling (continuous, uniform, sparse), and on the S/N of each measurement.

In the case of the *XMM-Newton*-COSMOS survey analyzed here, the light curve sampling is a worst case scenario as the fraction of time sampled is very small with respect to the total length of the light curves. However, we are sampling the low frequency part of the PSD, where the PSD slope is supposed to be flat ($\beta \sim 1$), and 80% of our sources have a total (0.5–10 keV) flux above $1 \times 10^{-14}$ erg cm$^{-2}$ s$^{-1}$. Therefore the average bias

---

[13] Defined as the ratio between the intrinsic $\sigma_{\rm rms}^2$ and the $\sigma_{\rm rms}^2$ observed with sparse sampling.
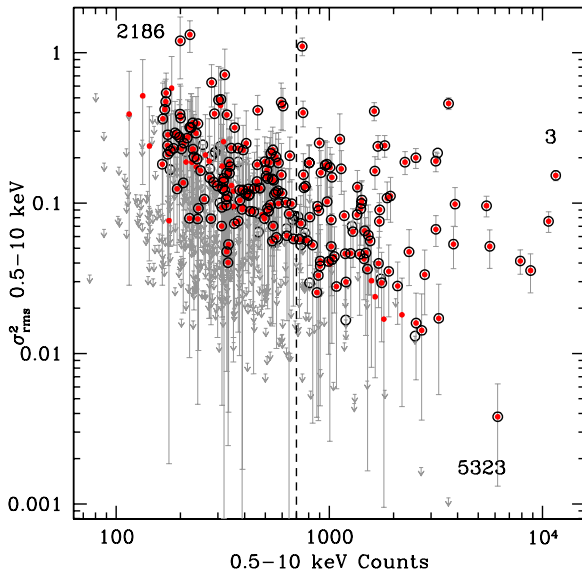
**Figure 6.** Distribution of $\sigma^2_{\rm rms}$ as a function of total net counts for each source. Sources with detection on $\sigma^2_{\rm rms}$ are labeled in red. Sources with an UL are in gray. Black circles mark sources considered variable on the basis of their $V$ parameter. The dashed line marks the 700 total net counts cut used in Section 5.1. The sources shown in Figure 3 are labeled with their XID.

(A color version of this figure is available in the online journal.)

factor is expected to be rather small ($\sim 1.2$). Nonetheless, the standard deviation of the distribution of bias factors is large. Therefore, the bias for a specific measurement can be very far from 1 for a significant fraction of sources. As a consequence, the $\sigma^2_{\rm rms}$ measured for a specific source should be taken cautiously. One way to overcome this problem is, however, to compute average $\sigma^2_{\rm rms}$ for samples of sources with similar properties. In this case, the scatter of the individual measurements around the average $\sigma^2_{\rm rms}$ can be used as the uncertainty on the average $\sigma^2_{\rm rms}$.

### 4.1. $\sigma^2_{rms}$ versus Counts

Figure 6 shows the distribution of the $\sigma^2_{\rm rms}$ as a function of total net counts for each source. Sources with a detection on $\sigma^2_{\rm rms}$ are labeled in red. Sources with an UL are in gray. Black circles mark sources considered variable on the basis of their $V$ parameter ($V > 1.3$). The distribution of $\sigma^2_{\rm rms}$ is in the log scale and ULs, defined as $\sigma^2_{\rm rms} + \sigma^2_{\rm rms\ Err}$, for all of the sources with $\sigma^2_{\rm rms}$-$\sigma^2_{\rm rms\ Err} < 0$ are reported. We note that all of the ULs are positive (i.e., $\sigma^2_{\rm rms} + \sigma^2_{\rm rms\ Err} > 0$).

There is clearly an anti-correlation between $\sigma^2_{\rm rms}$ and the number of counts. We emphasize that this anti-correlation is produced by the increasing minimum UL measurable for a given number of counts,[14] and hence the increasing minimum level at which we can have a detection, and by the fact that we have very few sources with high number of counts, hence the region with high $\sigma^2_{\rm rms}$ and high number of counts is less populated. The dashed line corresponds to the cut of 700 total net counts which we will use in Section 5.1 to evaluate the effect of the selection in $V$. We emphasize that above this line there is instead

no correlation between $\sigma^2_{\rm rms}$ and the number of counts, unlike what was found for the total sample.

If we assume that a detection in $\sigma^2_{\rm rms}$ can be considered as an indication of intrinsic variability, it is interesting to compare the distribution of $\sigma^2_{\rm rms}$ detections with that of sources showing $V > 1.3$. We recall, however, that the two methods express different concepts: the $V$ parameter indicates at which confidence a source can be considered variable, while the excess variance measures the amplitude of the variability. Nonetheless, the two methods give very similar results: There are only 21 sources detected in $\sigma^2_{\rm rms}$ which are non-variable according to the $V$ parameter and 36 sources variable in $V$ but not detected in $\sigma^2_{\rm rms}$. The agreement is also visually represented in Figure 6, where there is a high correspondence of red dots (detections in $\sigma^2_{\rm rms}$) and black circles ($V > 1.3$ sources).

### 5. $\sigma^2_{rms}$ VERSUS AGN PHYSICAL PROPERTIES

Due to the generally limited photon statistics of *XMM-COSMOS*, the majority of the sources in our sample have an UL on $\sigma^2_{\rm rms}$ because of the large errors associated with the small number of counts. We want to study how variability (namely $\sigma^2_{\rm rms}$) correlates with other quantities, such as $L_{0.5-10}$, z, BH mass, Eddington ratio, and optical properties, for sources for which we are able to constrain the quantity. Therefore, in the following we will first discuss such correlations for the subsample of 232 sources found to be significantly variable ($V > 1.3$), as was done in previous works (Paolillo et al. 2004; Papadakis et al. 2008; Young et al. 2012). However, we will also show that this selection criterion produces a strong bias in the distribution of $\sigma^2_{\rm rms}$, whereas selecting sources on the basis of the available number of counts produces more reliable results. We also note that the distributions of $\sigma^2_{\rm rms}$ for type 1 and type 2 sources are completely consistent. Therefore we will study the distribution of $\sigma^2_{\rm rms}$ as a function of other physical parameters for type 1 and type 2 together.

### 5.1. $\sigma^2_{rms}$ versus $L_{0.5-10}$ and z

Figure 7 (top) shows the distribution of $\sigma_{\rm rms}$ as a function of the 0.5–10 keV band luminosity for the sample of 232 sources with $V > 1.3$. The X-ray luminosities are corrected for absorption, either from spectral analysis (Mainieri et al. 2007) or hardness ratio (Brusa et al. 2010), and computed in the 0.5–10 keV rest-frame band. Blue squares are type 1 sources, red triangles are type 2, green crosses are galaxies. The dashed line represents the linear regression performed with the ASURV software Rev 1.2 (Isobe & Feigelson 1992), which implements the methods presented in Isobe et al. (1986). We adopted the results from the Buckley–James method, given that in all cases the censorship is present in only one variable. The results from the estimation maximization algorithm method are always consistent with those obtained with the Buckley–James method, while results from the Schmitt's binned linear regression are not suitable due to the limited number of data points. We excluded the two sources at $L_{0.5-10} < 10^{42}$ erg s$^{-1}$ from the fit, which may have significant contamination from the host galaxy. An anti-correlation between excess variance and X-ray luminosity is observed with high significance: the Spearman's rank correlation coefficient ($\rho_S = -0.375$) gives a probability of $P_S < 10^{-4}$. The resulting correlation is:

$$\log\left(\sigma^2_{\rm rms}\right) = (-0.91 \pm 0.02) + (-0.23 \pm 0.03)\log(L_{2-10\ {\rm keV},44})$$
(5)

with $L_{0.5-10}$ in units of $10^{44}$ erg s$^{-1}$.

---

[14] As for the variability index $V$, the ability to constrain the $\sigma_{\rm rms}$ depends strongly on the S/N (and hence number of counts) of each source. At $\gtrsim 3000$ counts we are able to detect excess variance values as small as $\sigma^2_{\rm rms} = 0.04$, while at lower counts the value of $\sigma^2_{\rm rms}$ must be much higher to be detected (e.g., >0.3 at $\sim$50 counts). The same is true for the minimum UL value, which changes from $\sim$0.001 above 3000 counts to $\sim$0.1 below 100 counts.

**Figure 7.** Left panel: distribution of $\sigma_{\rm rms}$ as a function of the 0.5–10 keV band intrinsic luminosity for the sample of sources with $V > 1.3$. Right panel: distribution of $\sigma_{\rm rms}$ as a function of redshift for sources with $V > 1.3$. In both panels the dashed line shows the linear regression including ULs for the total sample. The dotted lines show the errors in the coefficients. The black solid error bar shows the average error on $\sigma_{\rm rms}^2$. Blue squares are type 1 sources, red triangles are type 2, green crosses are galaxies.

(A color version of this figure is available in the online journal.)

A steeper anti-correlation for AGNs has been observed in previous works both for high frequencies (e.g., Barr & Mushotzky 1986; Lawrence & Papadakis 1993; Nandra et al. 1997; Hawkins 2000) and on longer time scales (Paolillo et al. 2004; Papadakis et al. 2008; Young et al. 2012). In particular, Paolillo et al. (2004) found a slope of $-1.31 \pm 0.23$ in the CDF-S, limiting the analysis to sources in the redshift range $0.5 < z < 1.5$. Papadakis et al. (2008) found a flatter slope of $-0.66 \pm 0.12$ in the Lockman Hole while Young et al. (2012) found a slope of $-0.76 \pm 0.06$ in the 4 Ms CDF-S data set (for sources with $L_{0.5-10} > 10^{42}$ erg s$^{-1}$), but not including sources with ULs. Again the latter sample is limited to $z \leqslant 1$.

Figure 7 (bottom) shows the distribution of $\sigma_{\rm rms}^2$ as a function of $z$ for the sample. No significant correlation is observed ($\rho_S = -0.031$ and $P_S = 0.6798$). This is somewhat unexpected, because at high redshift we are sampling the high luminosity part of the population and therefore we would expect to observe a decrease in the typical $\sigma_{\rm rms}^2$ with $z$. This is probably balanced by the fact that at high $z$ we are selecting a smaller fraction of variable sources (see Figure 4, right), thus selecting only the most variable ones.

The large redshift and $L_{0.5-10}$ range encompassed by the *XMM*-COSMOS survey allow us to study this issue more in detail. Figure 8 (top) shows the distribution of $\sigma_{\rm rms}^2$ versus $L_{0.5-10}$ for sources divided into three redshift bins ($z < 0.7$, $0.7 < z < 1.5$, and $1.5 < z < 3.5$). The dashed lines are linear regressions computed with ASURV for each subsample. Sources and lines are color coded so that blue represent the lower redshift sample, green the intermediate, and red the high redshift sample. Dividing the population in this way, the anti-correlation between $\sigma_{\rm rms}^2$ and $L_{0.5-10}$ is stronger: each correlation has $P_S < 10^{-4}$ and the slopes go from $-0.40 \pm 0.07$ to $-0.65 \pm 0.10$ from low to high redshift. Furthermore, it appears that for a given luminosity range and at all luminosities, the typical excess variance becomes higher at higher redshifts.

The intercept coefficients are significantly different, going from $-1.21 \pm 0.07$ to $-0.48 \pm 0.07$ from low to high redshift. An hint of a similar effect was observed in Paolillo et al. (2004), but the smaller sample size and $L_{0.5-10}$-$z$ coverage did not allow for a robust investigation in that work.

As explained in Section 4, due to the broad distribution of the bias introduced by measuring the excess variance from sparsely sampled light curves, the $\sigma_{\rm rms}^2$ measured for a specific source can be far from the intrinsic one. To overcome this problem, we computed the average excess variance for subsamples of sources showing similar physical properties (such as $L_{0.5-10}$, $z$, $M_{\rm BH}$, and Eddington ratio). Figure 8 (bottom) shows the distribution of average $\sigma_{\rm rms}^2$ versus $L_{0.5-10}$ for sources in the same redshift bins as the left panel and further binned in luminosity bins (one bin per decade). The positions of the squares mark the average of $\sigma_{\rm rms}^2$ and $L_{0.5-10}$ for the bin. The average is computed taking into account all of the values of $\sigma_{\rm rms}^2$ at face value for both detections and ULs (e.g., the computed value regardless of the errors, that for ULs can be negative). Error bars represent the standard error on the mean for both quantities in each subsample. The linear regressions of the left panel are shown for reference. We stress that the linear regressions computed with ASURV for the distribution of points in Figure 8 (top) are in perfect agreement with the distribution of the binned points.

We note that our decision to consider only the subsample of significantly variable sources ($V > 1.3$) avoids the difficulty of dealing with sparse light curves of faint sources for which the Poissonian noise is far greater than the intrinsic variability. However, we note that the $\langle \sigma_{\rm rms,V>1.3}^2 \rangle$ averaged over the subset of the sources with $V > 1.3$ is not the same as the $\langle \sigma_{\rm rms}^2 \rangle$ averaged over the whole set of sources and $\langle \sigma_{\rm rms,V>1.3}^2 \rangle$ will always be $\geqslant \langle \sigma_{\rm rms}^2 \rangle$. Therefore the selection $V > 1.3$ introduces a further bias in the averaged excess variances. The bias (in the estimation of the mean excess variance) is stronger the
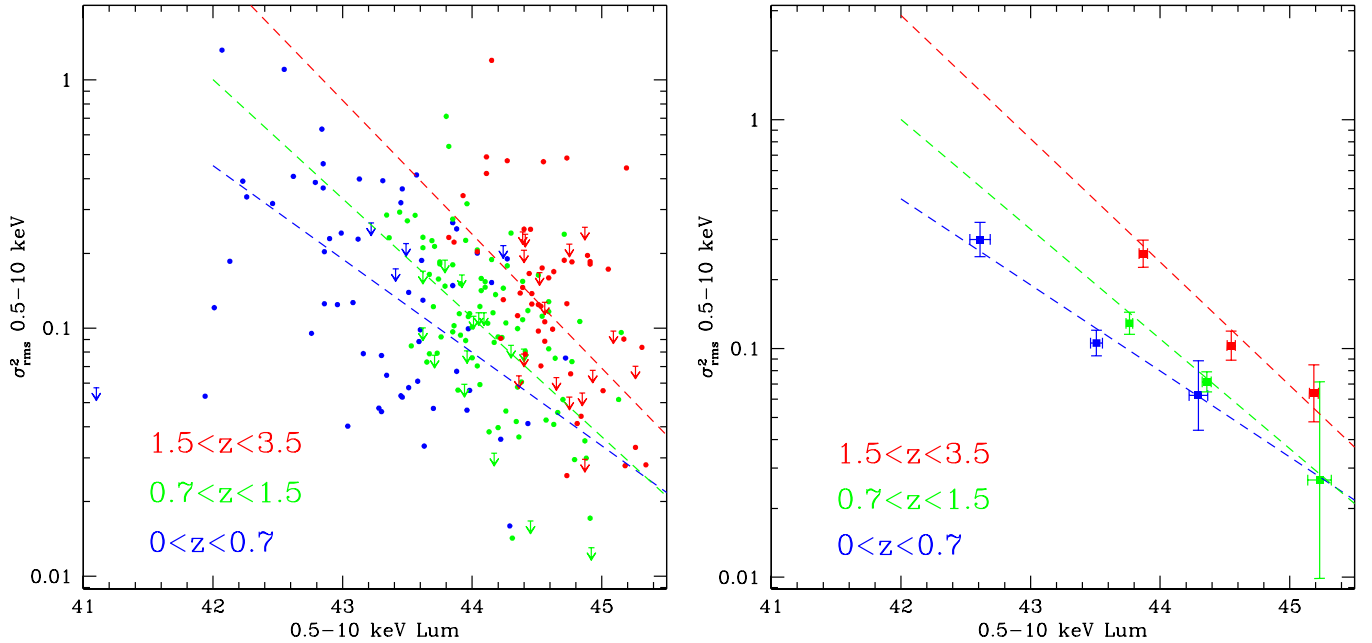
**Figure 8.** Left panel: same as Figure 7 (top), but here the sample has been divided into three redshift bins ($z < 0.7$, $0.7 < z < 1.5$, $1.5 < z < 4.5$). Sources and linear regressions are color coded so that blue represents the lower redshift sample, green the intermediate sample, and red the high redshift sample. Right panel: for each $z$ subsample, the average $\sigma^2_{\rm rms}$ and $L_{0.5-10}$ are shown in bins of luminosities. The squares mark the average of $\sigma^2_{\rm rms}$ and $L_{0.5-10}$ for the bin, while the error bars represent the standard error on the average. The same linear regressions obtained for the left panel are shown for reference.

(A color version of this figure is available in the online journal.)

larger the number of faint sources left out for each luminosity and $z$ bin.

From the light curves, we measure the variance ($S^2$) that has a contribution due to the intrinsic variability ($\sigma^2_{\rm rms}$) and the Poissonian noise ($\sigma^2_{\rm Poiss}$), $\sigma^2_{\rm rms} = S^2 + \sigma^2_{\rm Poiss}$ (Edelson et al. 2002). If, as in the majority of faint AGNs in *XMM*-COSMOS, $S^2 \sim \sigma^2_{\rm Poiss} \gg \sigma^2_{\rm rms}$, the uncertainty in the determination of the true value of $\sigma^2_{\rm Poiss}$ will lead to either an over- or underestimation of the excess variance, thus sometimes producing negative excess variances. The average of the excess variance estimates (considering both positive and negative values) is unbiased and it does tend to the real excess variance. On the other hand if, as done here, we average only the variable sources ($V > 1.3$) thus preferentially discarding the negative excess variance values, the obtained average excess variance will be overestimated, especially for those bins where a large fraction of faint sources are excluded. This is why we attribute the increasing observed AGN variability at high redshift (see Figure 8) to this effect. In fact, as shown in Section 3.3, the fraction of variable sources selected with a fixed values of $V$ decreases with redshift. This means that an increasingly large number of sources are left out from the bin when moving to high redshift.

To test this and to check how much of the observed effect is due to selection, we computed the same distribution of Figure 8 (bottom) in two cases. First (Figure 9, left), we included all the 638 sources with a light curve in the average distribution without any pre-selection. The linear regressions obtained in different redshift bins from Figure 8 are shown for reference. The average $\sigma^2_{\rm rms}$ for each bin is, as expected, lower than before, because we are including a large number of sources with $\sigma^2_{\rm rms}$ close to 0 (positive or negative) in the average and, as expected, the difference increases when moving to high redshift, because more sources were excluded at high redshift by the $V > 1.3$ selection (see Figure 4, right). Using the whole sample, the evolution in redshift is no longer significant.

Finally, we showed in Section 4 (and Figure 6) that the scatter in $\sigma^2_{\rm rms}$ increases when moving toward low counts due to light curves with poor statistics. We want to test the effect of this in the distribution of $\sigma^2_{\rm rms}$ and luminosity. Therefore, in Figure 9 (bottom) we selected sources on the basis of the number of counts available, i.e., sources with good statistics (>700 total net counts, 144 sources), for which we consider the estimation of variability to be more reliable. No selection in $V$ is used in this plot. Also, in this case all points are consistent with the local relation, i.e., that measured for $z < 0.7$:

$$\log(\sigma^2_{\rm rms}) = (-1.21 \pm 0.06) + (-0.40 \pm 0.07)\log(L_{2-10\,{\rm keV},44}) \tag{6}$$

even if the number of sources available for the bin is small and we are missing the low luminosity–high redshift bins. We underline that, even if the subsample used in Figure 9 (bottom) is much smaller than the one in Figure 9 (top), (144 sources instead of 638), the smaller scatter produce similar error bars.

These tests indicate that the selection based on the $V$ parameter introduces a bias at high redshift on the average excess variance. Once we average all of the excess variance values (with no selection in $V$), the evidence for higher AGN variability at high redshift is no longer significant for the *XMM*-COSMOS AGNs.

### 5.2. $\sigma_{\rm rms}$ versus $M_{BH}$ and $L_{Edd}$

We collected all of the BH mass information available to date in the *XMM*-COSMOS survey. For type 1 we have 89 virial masses available from Mg II from Merloni et al. (2010); 128 from Mg II, 31 from H$\beta$, and 37 from C IV from Trump et al. (2009); and 69 from H$\alpha$ and 183 from Mg II from Matsuoka et al. (2013). We also have a recompilation of these type 1 BH masses using the same spectra, but with a self consistent reanalysis, following Trakhtenbrot & Netzer (2012). The different BH mass values for sources with multiple measurements are in
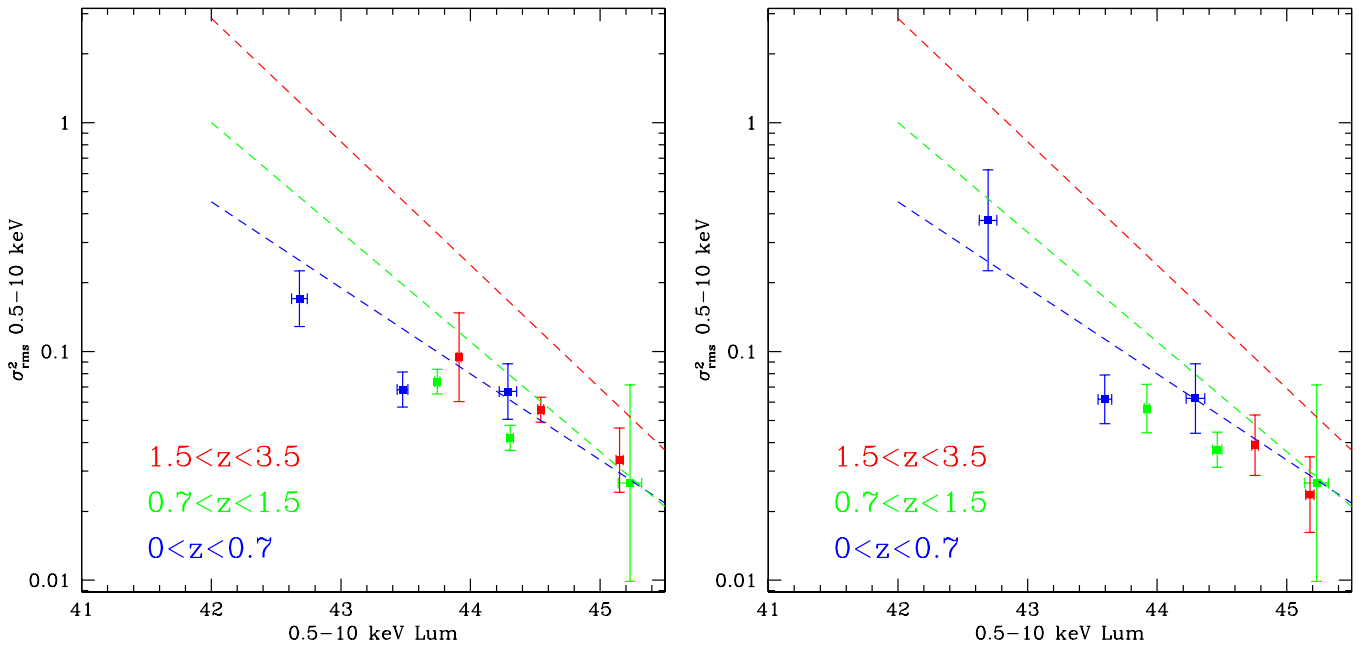
**Figure 9.** Left panel: $\sigma_{rms}^2$ vs. $L_{0.5-10}$ average distribution in redshift and $L_{0.5-10}$ bins for all of the 638 sources in the sample. The squares mark the average of $\sigma_{rms}^2$ and $L_{0.5-10}$ for the bin, while the error bars represent the standard error on the average. Right panel: same as top panel, but for sources selected on the basis of the number of counts available (>700 total net counts). In both panels the same linear regressions as those obtained for Figure 8 are shown for reference.

(A color version of this figure is available in the online journal.)

general in good agreement, within 0.3 dex. For type 2 we have 481 mass estimates through scaling relations and SED fitting from Lusso et al. (2011). In total we have at least one mass estimate for 814 sources.

As we already showed in Section 5, the less biased selection to study the dependency of $\sigma_{rms}^2$ on other physical properties in our sample requires selecting all sources (with no pre-selection in $V$). Furthermore, we chose to rely on the subsample of sources with sufficiently good statistics (>700 counts) for which the estimation of variability is more reliable. Using the same selection, we built a sample of 111 sources with $M_{BH}$ estimates. We stress that this is the first time that the correlation between X-ray variability on long time scales and BH masses can be performed in such large sample of AGNs spanning a wide range of redshift.

The distribution of excess variance as a function of the BH mass is shown in Figure 10 (top). Single sources are shown in gray (squares for type 1 and triangles for type 2). The black error bar shows the average (representative of a single measurement) error on $\sigma_{rms}^2$. The position of the filled blue squares mark the average of $\sigma_{rms}^2$ and $M_{BH}$ in five bins of BH mass, where sources with ULs are also taken into account with their nominal value. Error bars represent the standard error on the mean for both quantities in each subsample.

When only sources with good statistics are considered, the correlation between $\sigma_{rms}^2$ and $M_{BH}$ is strong ($\rho_S = -0.315$ and $P_S = 0.0007$), with a slope of $-0.42 \pm 0.11$. We note that the correlation between $\sigma_{rms}^2$ and the $M_{BH}$ found in previous works sampling higher frequencies (minutes–hours) is of the order of $-1$ (e.g., P12). This is generally interpreted with the fact that the $\sigma_{rms}^2$, measuring the integral of the PSD in that specific frequency rangem is affected by the position of $\nu_b$ which scales linearly with the BH mass.

The lower frequencies sampled in the *XMM*-COSMOS survey are in the months–years regime. On the other hand, the highest frequency sampled by a sparsely sampled light curve is not

well defined. However, in most light curves the minimum distance between two observations is of the order of hours–days. Therefore we are integrating the PSD both above and below $\nu_b$. The part of the PSD integral above $\nu_b$ would introduce a linear correlation of the excess variance with $M_{BH}$, but this is weakened by the part of the integral below $\nu_b$ which would induce no correlation (see for example Soldi et al. 2013).

We also collected the AGN bolometric luminosities from Lusso et al. (2010) for type 1 (estimated from direct integration of the rest-frame SED) and Lusso et al. (2011) for type 2 (from SED-fitting by assuming a fixed covering factor of 0.67). Thanks to this, we were able to compute Eddington ratios for 74 sources with >700 counts.

Figure 10 (bottom) shows the distribution of $\sigma_{rms}^2$ as a function of Eddington ratio expressed as $L_{Bol}/L_{Edd}$. As in Figure 10 (top), gray points show single sources, blue filled squares represent the average of $\sigma_{rms}^2$ and $L_{Bol}/L_{Edd}$ in five bins of Eddington ratio. There is no correlation between $\sigma_{rms}^2$ and the Eddington ratio ($\rho_S = -0.122$ and $P_S = 0.2784$, with a slope fully consistent with 0, $-0.09 \pm 0.14$).

It is also interesting to note that the slope of the $\sigma_{rms}^2$ versus $M_{BH}$ in Figure 10 (top) is the same as that of the global slope between $\sigma_{rms}^2$ and $L_{0.5-10}$ in Figure 9 (bottom). This suggests that the latter is a by-product of the former one, as observed at lower frequencies (P12). This is shown if Figure 11 where the distribution of $\sigma_{rms}^2$ versus $L_{0.5-10}$ is shown for sources with >700 counts after normalizing $\sigma_{rms}^2$ for the $M_{BH}$. The linear regression between the $\sigma_{rms}^2$ normalized for the BH mass is fully consistent with 0 (slope of $0.13 \pm 0.12$).

The residual scatter of $\sigma_{rms}^2$ after accounting for the $M_{BH}/L_{0.5-10}$ dependency is still of $\sim 2$ orders of magnitude for individual values. This would imply that the normalization PSD below $\nu_b$ is not the same for all of the sources as is usually assumed. However, as we pointed out in Section 5.1, it has been shown in Allevato et al. (2013) that the bias due to sparse sampling can be broadly distributed between 0.1 and 10,
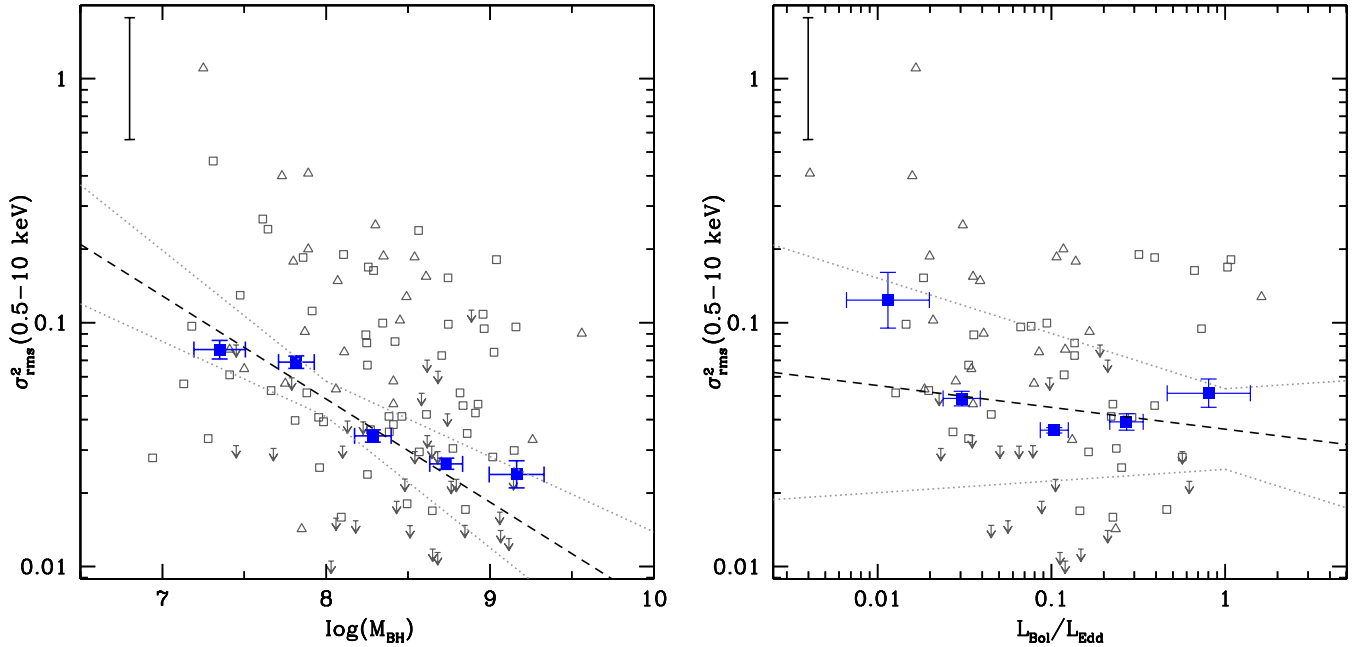
**Figure 10.** Left panel: distribution of $\sigma^2_{\rm rms}$ as a function of the BH masses for sources with more than 700 total net counts and no selection in the V parameter. Right panel: distribution of $\sigma^2_{\rm rms}$ as a function of Eddington ratio, expressed as $L_{\rm Bol}/L_{\rm Edd}$, for the same sample. In both panels the dashed line shows the linear regression including ULs. The dotted lines show the errors in the coefficients. The black solid error bar shows the average error on $\sigma^2_{\rm rms}$. Blue squares are type 1 sources, red triangles are type 2, green crosses are galaxies.

(A color version of this figure is available in the online journal.)
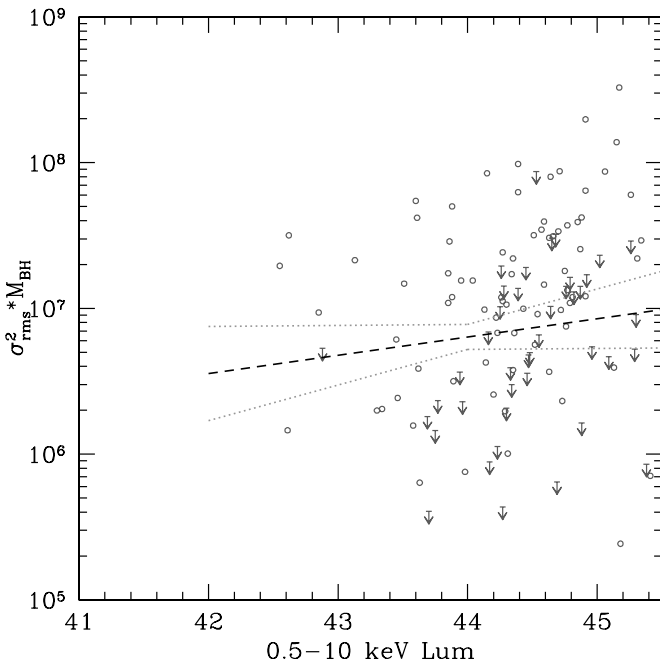


**Figure 11.** Distribution of $\sigma^2_{\rm rms} * M_{\rm BH}$ for sources with more than 700 total net counts. The linear regression computed for $\sigma^2_{\rm rms}$ normalized for the BH mass is consistent with 0.

meaning that we cannot use the observed scatter of individual $\sigma^2_{\rm rms}$ values as a direct probe for the intrinsic scatter of the PSD normalization.

The existence of the correlation between $\sigma^2_{\rm rms}$ and Eddington ratio is debated in the literature (O'Neill et al. 2005; McHardy et al. 2006; Körding et al. 2007; P12). At low frequencies, Young et al. (2012) found a significant anti-correlation between $\sigma^2_{\rm rms}$ and accretion rate which they interpreted as an artifact of

the $\sigma^2_{\rm rms} - L_{0.5-10}$ anti-correlation. In our dataset the correlation is globally flat. A hint of bi-modality is present in Figure 10 (bottom), with average $\sigma^2_{\rm rms}$ increasing both for very high and very low accretion rates. However the quality of the data and the limited sample included here do not allow further investigation of this issue.

### 5.3. Optical versus X-Ray Variability

The optical variability, expressed in $\Delta$mag, was computed in Salvato et al. (2009; see details in Section 3 of that paper for the definition of $\Delta$mag) in order to correct for its effect when computing photometric redshifts. The COSMOS optical photometry has been acquired in five epochs distributed over ∼6 yr. Within each epoch (apart from 2005), several individual filter observations were distributed over less than three months, covering the whole optical range. This allowed AGN time variability to be studied and corrected over time scales of years, while shorter variability cannot easily be addressed. A source with $\Delta$Mag > 0.25 was considered variable.

The optical variability is show in Figure 12 (top) as a function of the X-ray $\sigma^2_{\rm rms}$ for sources with $V > 1.3$. The two quantities are clearly not correlated ($\rho_S = -0.113$ and $P_S = 0.0611$). The optical photometry is not simultaneous to the X-ray observations but span a larger time scale. Also the cadence is different. These two factors (in addition to the variability being produced at various distances from the BH, depending on the wavelength) can explain why X-ray and optical variability are not clearly correlated.

Figure 13 reports two examples of sources that are highly variable in one band and not in the other. Source 2016 (top) is a source classified as broad line from the optical spectrum and it is non-variable in X-ray and highly variable in optical. Source 5192 (bottom), classified as type 2 from the SED fitting, is instead variable in X-ray while showing a perfectly flat optical light curve.
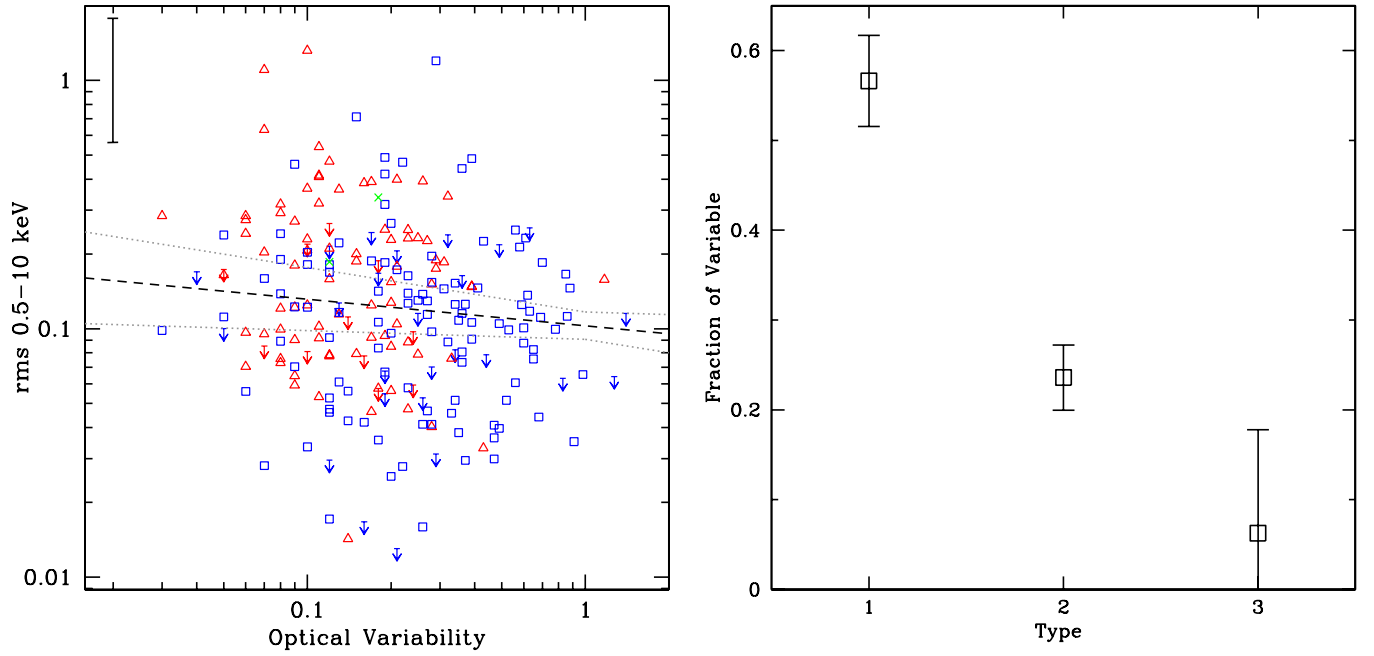
**Figure 12.** Left panel: distribution of optical vs. X-ray variability for all of the sources with $V > 1.3$. Right panel: fraction of Optically variable sources, divided by optical type.

(A color version of this figure is available in the online journal.)
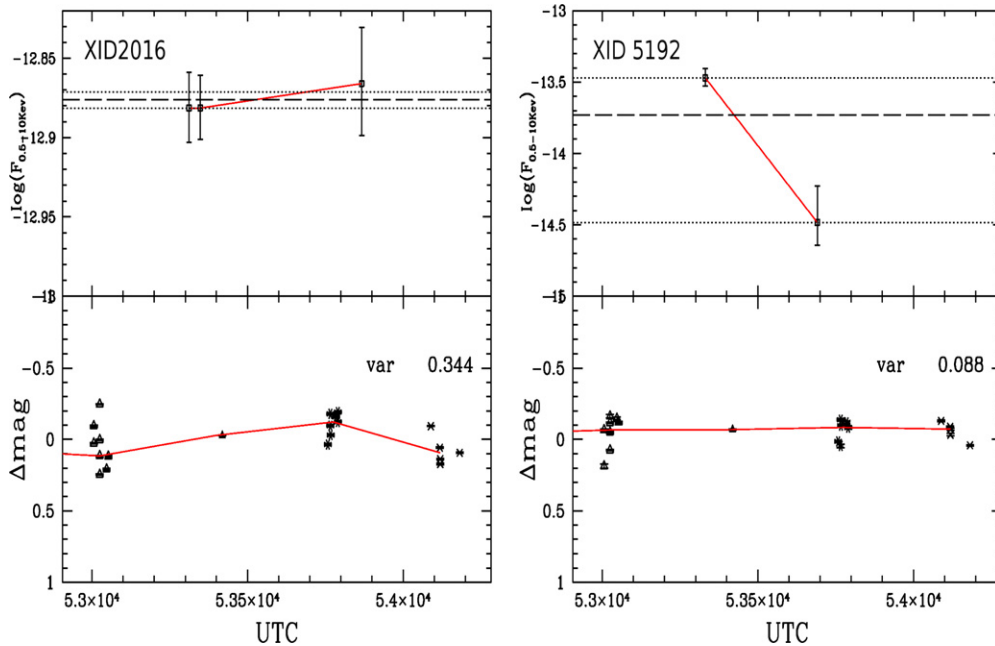


**Figure 13.** Top panels: *XMM-Newton* 0.5–10 keV, background subtracted light curve of XID #2016 and 5192. The dashed line shows the weighted mean of the 0.5–10 keV flux. Dotted lines show the standard error on the mean. The continuous line connects data points. Bottom panels: the sources were observed in four epochs, each epoch marked with a different symbol as in Figure 3. The red line connects the median values of the deviation from a running Gaussian filter for each group of observations. The points in each group refer to different wavelengths, therefore the differences within points in each group are due to the SED shape and not variability.

(A color version of this figure is available in the online journal.)

Finally, optical variability tends to be highly type-dependent (Figure 12, right): the fraction of type 1 that is optically variable ($\Delta$Mag $> 0.25$ Mag) is considerably higher ($\sim$55%) than that of type 2 ($\sim$25%). We underline, however, that variability is one of the criteria that is used in the process to identify sources with photometric redshift as AGN-dominated or galaxy-dominated (see flow chart in Figure 6 of Salvato et al. (2011) for details on the template class assignation), thus this result is partly an induced effect.

## 6. CONCLUSIONS

We used the repeated *XMM-Newton* observations in the COSMOS field to study the long term (months–years in the rest-frame) variability of a large sample of X-ray detected AGNs. We found as follows.

1. Variability is prevalent in AGNs whenever we have good statistics to measure it. (up to 75% of variable sources in the $>1000$ counts regime);

2. There is no significant difference in the distribution of variability between type 1 and type 2 sources.

3. The anti-correlation between $\sigma_{\rm rms}^2$ and $L_{0.5-10}$ has a rather flat slope ($\alpha = -0.25$) when the total sample of variable sources ($V > 1.3$) is considered. If the sample is divided into redshift bins however, a steeper anti-correlation is observed in all bins, with both slope and normalization increasing with redshift.

4. The previous result is affected by two main selection effects: the selection in $V$ and the correlation between $\sigma_{\rm rms}^2$ and counts, both producing higher average $\sigma_{\rm rms}^2$ at low $L_{0.5-10}$ and high $z$. If all of the sources with good statistics ($>700$ counts) and only those sources are considered, the evolution in $z$ of the $\sigma_{\rm rms}^2 - L_{0.5-10}$ relation is no longer significant and the relation at low redshift ($z < 0.7$) with a slope of $-0.40 \pm 0.06$ perfectly fits the remaining data points.

5. Thanks to the wealth of data available in the COSMOS field, for the first time we were able study the correlation between long term X-ray variability, BH masses, and Eddington ratios in a large sample of AGNs. If only sources with more than 700 counts are considered, a strong anti-correlation between $M_{\rm BH}$ and $\sigma_{\rm rms}^2$ is observed ($\rho_S = -0.315$ and slope of $-0.42 \pm 0.11$), while no correlation is found between $L_{\rm Bol}/L_{\rm Edd}$ and $\sigma_{\rm rms}^2$.

6. The anti-correlation between $\sigma_{\rm rms}^2$ and $L_{0.5-10}$ disappears if $\sigma_{\rm rms}^2$ is normalized for the $M_{\rm BH}$, suggesting that the anti-correlation with luminosity is the by-product of the more intrinsic anti-correlation with $M_{\rm BH}$.

7. No clear correlation is found between the optical and the X-ray variability.

The study of long term variability in large samples of high redshift AGNs will further benefit in the near future from the ongoing extension of the X-ray coverage in the COSMOS field with *Chandra* (The COSMOS Legacy Survey, PI: Civano), and from the extra 3 Ms of observation in the *Chandra*-DFS, awarded in Cycle 15 (PI: Brandt).

## REFERENCES

Allevato, V., Paolillo, M., Papadakis, I., & Pinto, C. 2013, ApJ, 771, 9
Axelsson, M., Borgonovo, L., & Larsson, S. 2005, A&A, 438, 999
Barr, P., & Mushotzky, R. F. 1986, Natur, 320, 421
Beckmann, V., Barthelmy, S. D., Courvoisier, T., et al. 2008, in Proc. AAS/High Energy Astrophysics Division, 10, 26.02
Bonoli, F., Braccesi, A., Federici, L., Zitelli, V., & Formiggini, L. 1979, A&AS, 35, 391
Brusa, M., Civano, F., Comastri, A., et al. 2010, ApJ, 716, 348
Caballero-Garcia, M. D., Papadakis, I. E., Nicastro, F., & Ajello, M. 2012, A&A, 537, A87
Capak, P., Aussel, H., Ajiki, M., et al. 2007, ApJS, 172, 99
Cappelluti, N., Brusa, M., Hasinger, G., et al. 2009, A&A, 497, 635
Czerny, B., Nikolajuk, M., Piasecki, M., & Kuraszkiewicz, J. 2001, MNRAS, 325, 865
de Vries, W. H., Becker, R. H., White, R. L., & Loomis, C. 2005, AJ, 129, 615
Edelson, R., & Nandra, K. 1999, ApJ, 514, 682
Edelson, R., Turner, T. J., Pounds, K., et al. 2002, ApJ, 568, 610
Edelson, R. A., Krolik, J. H., & Pike, G. F. 1990, ApJ, 359, 86
Gallo, L. C., Brandt, W. N., Costantini, E., et al. 2007, MNRAS, 377, 391
George, I. M., Turner, T. J., Yaqoob, T., et al. 2000, ApJ, 531, 52
Giallongo, E., Trevese, D., & Vagnetti, F. 1991, ApJ, 377, 345
Gierliński, M., Nikolajuk, M., & Czerny, B. 2008, MNRAS, 383, 741
González-Martín, O., & Vaughan, S. 2012, A&A, 544, A80
Green, A. R., McHardy, I. M., & Lehto, H. J. 1993, MNRAS, 265, 664
Hasinger, G., Cappelluti, N., Brunner, H., et al. 2007, ApJS, 172, 29
Hawkins, M. R. S. 2000, A&AS, 143, 465
Hayashida, K., Miyamoto, S., Kitamoto, S., Negoro, H., & Inoue, H. 1998, ApJ, 500, 642
Ilbert, O., Capak, P., Salvato, M., et al. 2009, ApJ, 690, 1236
Isobe, T., & Feigelson, E. D. 1992, ApJS, 79, 197
Isobe, T., Feigelson, E. D., & Nelson, P. I. 1986, ApJ, 306, 490
Kelly, B. C., Sobolewska, M., & Siemiginowska, A. 2011, ApJ, 730, 52
Körding, E. G., Migliari, S., Fender, R., et al. 2007, MNRAS, 380, 301
Lawrence, A., & Papadakis, I. 1993, ApJL, 414, L85
Lilly, S. J., Le Brun, V., Maier, C., et al. 2009, ApJS, 184, 218
Lusso, E., Comastri, A., Simmons, B. D., et al. 2012, MNRAS, 425, 623
Lusso, E., Comastri, A., Vignali, C., et al. 2010, A&A, 512, A34
Lusso, E., Comastri, A., Vignali, C., et al. 2011, A&A, 534, A110
Mainieri, V., Hasinger, G., Cappelluti, N., et al. 2007, ApJS, 172, 368
Markowitz, A., & Edelson, R. 2004, ApJ, 617, 939
Matsuoka, K., Silverman, J. D., Schramm, M., et al. 2013, ApJ, 771, 64
McHardy, I. M., Koerding, E., Knigge, C., Uttley, P., & Fender, R. P. 2006, Natur, 444, 730
McLaughlin, M. A., Mattox, J. R., Cordes, J. M., & Thompson, D. J. 1996, ApJ, 473, 763
Merloni, A., Bongiorno, A., Bolzonella, M., et al. 2010, ApJ, 708, 137
Nandra, K., George, I. M., Mushotzky, R. F., Turner, T. J., & Yaqoob, T. 1997, ApJ, 476, 70
O'Neill, P. M., Nandra, K., Papadakis, I. E., & Turner, T. J. 2005, MNRAS, 358, 1405
Paolillo, M., Schreier, E. J., Giacconi, R., Koekemoer, A. M., & Grogin, N. A. 2004, ApJ, 611, 93
Papadakis, I. E. 2004, MNRAS, 348, 207
Papadakis, I. E., Chatzopoulos, E., Athanasiadis, D., Markowitz, A., & Georgantopoulos, I. 2008, A&A, 487, 475
Papadakis, I. E., & McHardy, I. M. 1995, MNRAS, 273, 923
Ponti, G., Cappi, M., Dadina, M., & Malaguti, G. 2004, A&A, 417, 451
Ponti, G., Papadakis, I., Bianchi, S., et al. 2012, A&A, 542, A83
Rees, M. J. 1984, ARA&A, 22, 471
Salvato, M., Hasinger, G., Ilbert, O., et al. 2009, ApJ, 690, 1250
Salvato, M., Ilbert, O., Hasinger, G., et al. 2011, ApJ, 742, 61
Sarajedini, V. L., Koo, D. C., Klesman, A. J., et al. 2011, ApJ, 731, 97
Scoville, N., Aussel, H., Brusa, M., et al. 2007, ApJS, 172, 1
Soldi, S., Baumgartner, W., Beckmann, V., et al. 2011, in Proc. The X-ray Universe 2011, 154
Soldi, S., Beckmann, V., Baumgartner, W. H., et al. 2013, arXiv:1311.4164
Trakhtenbrot, B., & Netzer, H. 2012, MNRAS, 427, 3081
Trevese, D., Boutsia, K., Vagnetti, F., Cappellaro, E., & Puccetti, S. 2008, A&A, 488, 73
Trevese, D., Kron, R. G., Majewski, S. R., Bershady, M. A., & Koo, D. C. 1994, ApJ, 433, 494
Trump, J. R., Impey, C. D., McCarthy, P. J., et al. 2007, ApJS, 172, 383
Trump, J. R., Impey, C. D., Taniguchi, Y., et al. 2009, ApJ, 706, 797
Turner, T. J., George, I. M., Nandra, K., & Turcan, D. 1999, ApJ, 524, 667
Uttley, P., McHardy, I. M., & Papadakis, I. E. 2002, MNRAS, 332, 231
Vanden Berk, D. E., Wilhite, B. C., Kron, R. G., et al. 2004, ApJ, 601, 692
van den Bergh, S., Herbst, E., & Pritchet, C. 1973, AJ, 78, 375
Vaughan, S., Edelson, R., Warwick, R. S., & Uttley, P. 2003, MNRAS, 345, 1271
Vaughan, S., & Fabian, A. C. 2004, MNRAS, 348, 1415
Villforth, C., Koekemoer, A. M., & Grogin, N. A. 2010, ApJ, 723, 737
Young, M., Brandt, W. N., Xue, Y. Q., et al. 2012, ApJ, 748, 124
Zhang, Y.-H. 2011, ApJ, 726, 21
Zhou, X.-L., Zhang, S.-N., Wang, D.-X., & Zhu, L. 2010, ApJ, 710, 16